Cancer Science

WILEY

Cancer Science

ORIGINAL ARTICLE OPEN ACCESS

Quantitative Live Imaging Reveals Phase Dependency of PDAC Patient-Derived Organoids on ERK and AMPK Activity

Shoko Tsukamoto[1] | Ye Huaze[2] | Zhang Weisheng[2] | Akihito Machinaga[3] | Nobuyuki Kakiuchi[4,5] | Seishi Ogawa[6] | Hiroshi Seno[5] | Shigeki Higashiyama[7] | Michiyuki Matsuda[1,8] | Toru Hiratsuka[2,7]

[1]Laboratory of Cell Cycle Regulation, Graduate School of Biostudies, Kyoto University, Kyoto, Japan | [2]Department of Molecular Oncology, Graduate School of Medicine, Osaka University, Osaka, Japan | [3]Oncology Tsukuba Research Department, Discovery, Medicine Creation, OBG, Eisai Co. Ltd., Tsukuba, Japan | [4]Department of Gastroenterology and Hepatology, Graduate School of Medicine, Kyoto University, Kyoto, Japan | [5]The Hakubi Center for Advanced Research, Kyoto University, Kyoto, Japan | [6]Department of Pathology and Tumor Biology, Graduate School of Medicine, Kyoto University, Kyoto, Japan | [7]Department of Oncogenesis and Growth Regulation, Research Center, Osaka International Cancer Institute, Osaka, Japan | [8]Affiliated Graduate School, Graduate School of Medicine, Kyoto University, Kyoto, Japan

Correspondence: Toru Hiratsuka (toru.hiratsuka@oici.jp)

Received: 24 August 2024 | **Revised:** 6 December 2024 | **Accepted:** 12 December 2024

Funding: This work was supported by JST Moonshot R&D Program, Grant Number JPMJMS2022, The Japan Agency for Medical Research and Development (AMED) Core Research for Evolutional Science and Technology (CREST), Grant Number 23gm1110011h0005, AMED Moonshot Research and Development Program, Grant Number 24zf0127009h0003, Japan Society for the Promotion of Science (JSPS) KAKENHI Grant-in-Aid for Scientific Research (S), Grant Number 15H05909, JSPS KAKENHI Grant-in-Aid for Specially Promoted Research, Grant Number 24H00009, JSPS KAKENHI Grant-in-Aid for Scientific Research (C) Number 24K10301, JSPS KEKENHI Grant-in-Aid for Early Career Scientists Number 22K15510, Konica Minolta Imaging Science Encouragement Award, The Mitsubishi Foundation, and JST SPRING, Grant Number JPMJSP2110.

Keywords: AMPK | ERK | heterogeneity | live imaging | pancreatic cancer

ABSTRACT

Patient-derived organoids represent a novel platform to recapitulate the cancer cells in the patient tissue. While cancer heterogeneity has been extensively studied by a number of omics approaches, little is known about the spatiotemporal kinase activity dynamics. Here we applied a live imaging approach to organoids derived from 10 pancreatic ductal adenocarcinoma (PDAC) patients to comprehensively understand their heterogeneous growth potential and drug responses. By automated wide-area image acquisitions and analyses, the PDAC cells were non-selectively observed to evaluate their heterogeneous growth patterns. We monitored single-cell ERK and AMPK activities to relate cellular dynamics to molecular dynamics. Furthermore, we evaluated two anti-cancer drugs, a MEK inhibitor, PD0325901, and an autophagy inhibitor, hydroxychloroquine (HCQ), by our analysis platform. Our analyses revealed a phase-dependent regulation of PDAC organoid growth, where ERK activity is necessary for the early phase and AMPK activity is necessary for the late stage of organoid growth. Consistently, we found PD0325901 and HCQ target distinct organoid populations, revealing their combination is widely effective to the heterogeneous cancer cell population in a range of PDAC patient-derived organoid lines. Together, our live imaging quantitatively characterized the growth and drug sensitivity of human PDAC organoids at multiple levels: in single cells, single organoids, and individual patients. This study will pave the way for understanding the cancer heterogeneity and promote the development of new drugs that eradicate intractable cancer.

1 | Introduction

Pancreatic ductal adenocarcinoma (PDAC) is one of the most malignant cancers, with its 5-year survival rate being around 10% [1]. Because of the high prevalence of oncogenic mutation of KRAS gene (> 90%) [2], ERK (extracellular signal-regulated kinase) signaling pathway has been the central drug target of PDAC [3]. Despite the development of numerous drugs targeting the signal pathway [4–13], most chemicals did not show significant efficacy in clinical trials, which includes, SOS inhibitor [14], MEK inhibitors [15–18], and ERK inhibitor [19].

Cellular autophagy signal is enhanced in KRAS mutant PDAC cells [20]. Autophagy activation correlates with shorter disease-free periods in patients [21] and an autophagy inhibitor, hydroxychloroquine (HCQ) suppressed tumor growth in a PDAC mouse model [22]. However, a clinical study showed that HCQ monotherapy has limited efficacy [23]. Recently, combination therapies targeting autophagy and growth signaling pathways have emerged as a promising strategy to synergistically suppress malignant cancer [24–26].

Organoid culture of patient-derived cancer cells is a novel culture system that mimics cancer cells in the human tissue [27–31]. Studies show PDAC organoids of different transcriptional signatures have varied drug responses [28, 32–36], and the drug efficacy correlates with the prognosis of the patients [33, 34]. However, the heterogeneous feature of organoids proposes technical challenges as an experimental model. Individual tumors are heterogenous at the histological, genomic, and transcriptomic levels [37–39]. Besides, tumor heterogeneity dynamically changes by time [40]. While multiple omics approaches revealed single-cell heterogeneity [29, 40–43], its temporal changes need to be complemented by live imaging approaches.

Here, we applied a live imaging approach to 10 PDAC patient-derived organoids to investigate the activity of ERK and AMP-activated protein kinase (AMPK) as proxies of cell growth and autophagy signal. Our quantitative analysis revealed the spatio-temporal landscape of human PDAC cells and phase-dependent roles of ERK and AMPK activity in the organoid growth. We show that the combination of the two targets is effective in a wide range of human PDAC organoid lines.

2 | Materials and Methods

2.1 | Plasmids

The lentiviral plasmid for EKAREN5 is a kind gift from Dr. Hugo Snippert (University Medical Center Utrecht, Addgene 167823). EKAREN5-gl-NLS and EKAREN5-gl-NLS-TA were reported previously [44]. The synonymous codon variant YPet cassette was obtained from EKARrEV-NLS [45] by PCR. AMPKAR-EV plasmid was previously published [46]. These biosensors were subcloned into pCSII lentiviral backbone (RIKEN).

2.2 | FRET Imaging of HeLa Cells Expressing EKAREN5-gl-NLS

HeLa cells were purchased from the Human Science Research Resources Bank and maintained in DMEM containing 10% FBS (Sigma-Aldrich). HeLa cells expressing EKAREN5-gl-NLS were plated onto an 8-well chamber (IWAKI) coated with 150 μg/mL collagen solution. Following starvation for 1 h in FluoroBright DMEM (gibco) supplemented with 2 mM L-glutamine, the cells were observed by FV10i laser scanning confocal microscope (Evident). Images were acquired by preset dye settings of ECFP and EYFP in Fluoview software.

2.3 | PDAC Organoid Culture

PDAC organoids were established under the approval from Kyoto University Certified Review Board and Kyoto University Graduate School and Faculty of Medicine, Ethics Committee (G0738) and cultured in Matrigel (Corning, 356231) with organoid culture complete medium, which is phenol red-free DMEM/F-12 medium (Thermo Fisher Scientific) supplemented with 10 mM HEPES (Thermo Fisher Scientific), 500 μM Sodium Pyruvate (Thermo Fisher Scientific), Penicillin–Streptomycin (Nacalai tesque), 2 mM GlutaMax (Thermo Fisher Scientific), 100 ng/mL Wnt-3a (R&D Systems), 500 ng/mL R-spondin 1 (R&D Systems), 100 ng/mL Noggin (R&D Systems), 100 ng/mL FGF-10 (Pepro Tech), 50 ng/mL EGF (Pepro Tech), 10 nM Gastrin I human (Sigma-Aldrich), 500 nM A-83-01 (FUJIFILM Wako Pure Chemical Corporation), 1x B-27 Supplement (Thermo Fisher Scientific, 17504044), 10 mM Nicotinamide (Sigma-Aldrich), and 1 mM N-acetyl-L-cysteine (Sigma-Aldrich).

2.4 | Lentivirus Production and Infection

Lenti-X 293T cells (Clontech) were cultured in DMEM (FUJIFILM Wako Pure Chemical Corporation) supplemented with 10% FBS (Nichirei) and 1% Penicillin–Streptomycin. Lenti-X 293T cells were co-transfected with pCSII lentiviral plasmid, pCMV-VSV-G-RSV-Rev (RIKEN) and psPAX2 (Addgene 12260). After 2 days of incubation, viruses were collected and concentrated by PEG6000. For lentivirus infection, the concentrated virus particles were added to the organoid culture together with 10 μM Y27632 and 10 μg/mL polybrene (Nacalai tesque) and centrifuged at 600 *g* for 60 min.

2.5 | Microscopy

Phase contrast images (Figure 1A) of cultured organoids were acquired by Axiovert 25 microscope (Carl Zeiss) with 20×/0.30 NA dry objective lens (Carl Zeiss) and Digital single lens reflex camera D5100 (Nikon).

For two-photon microscope observation, an Olympus LV110-MPE incubator microscope equipped with InSight DeepSee

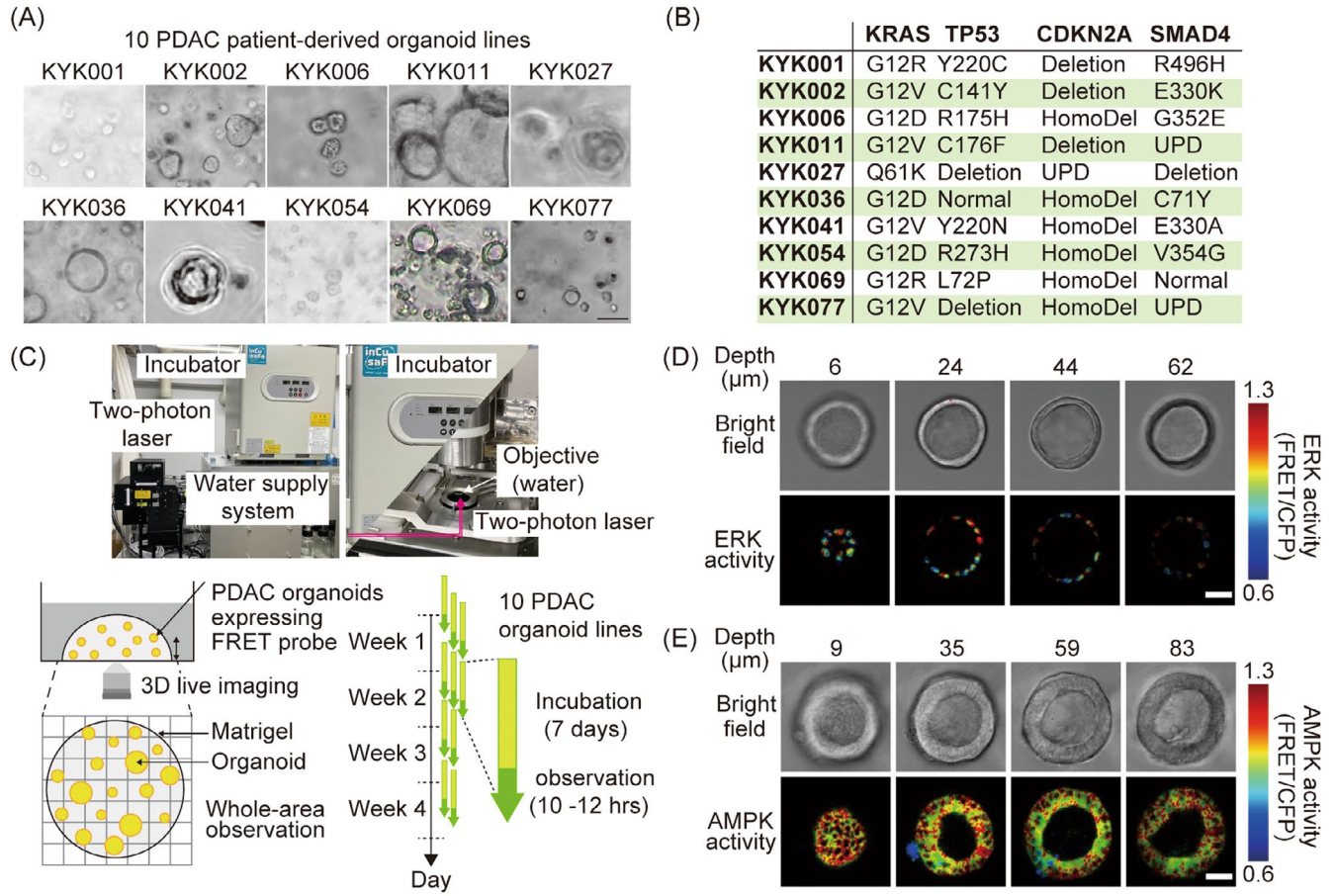

	KRAS	TP53	CDKN2A	SMAD4
KYK001	G12R	Y220C	Deletion	R496H
KYK002	G12V	C141Y	Deletion	E330K
KYK006	G12D	R175H	HomoDel	G352E
KYK011	G12V	C176F	Deletion	UPD
KYK027	Q61K	Deletion	UPD	Deletion
KYK036	G12D	Normal	HomoDel	C71Y
KYK041	G12V	Y220N	HomoDel	E330A
KYK054	G12D	R273H	HomoDel	V354G
KYK069	G12R	L72P	HomoDel	Normal
KYK077	G12V	Deletion	HomoDel	UPD

FIGURE 1 | Live imaging strategy for PDAC patient-derived organoid lines. (A) Bright-field images of 10 human PDAC organoid lines (KYK organoids). Scale bar, 50 μm. (B) Genetic profile of the KYK organoid lines. UPD: Uniparental disomy, HomoDel: Homozygous deletion. (C) Photos of the incubator two-photon microscope (above) and schematics of the experimental set-up (below). (D, E) Bright-field images and intensity-modulated display (IMD) images of ERK activity (FRET/CFP) in PDAC organoids expressing EKAREN5-gl-NLS (D) or AMPKAR-EV (E). Numbers indicate the relative depth from the top of the organoid.

Laser (Spectra-Physics) and an IR-cut filter (Olympus, 32BA750RIF) was used. We used a 25×/1.05 NA water objective lens (Olympus, XLPLN25XWMP2) and the 840 nm laser for the excitation of FRET probes. For CFP signals, dichroic mirrors (Olympus, SDM505, and RDM445XL) and an emission filter (Olympus, 32BA460-500) were used. For FRET signals, dichroic mirrors (Olympus, SDM505, and SDM570) and an emission filter (Olympus, 32BA520-560) were used.

For confocal observation and fluorescence lifetime imaging, TCS SP8 X FALCON (Leica Microsystems) equipped with a Pulsed Diode Laser (PicoQuant, PDL 800-D) was used. We used an HCPL APO 20×/0.75 CS2 dry lens (Leica Microsystems, 11506517), and 440 nm laser was used to excite the FRET probes. CFP signals and FRET signals were detected by Leica HyD detector (Leica Microsystems) (CFP: 459–487 nm, FRET: 512–534 nm).

2.6 | Microscopic Observation of PDAC Organoids

For live imaging, 1000 cells were seeded on a grass-bottom 96 well plate (Iwaki). 63 Z slices were acquired with a 3 μm step for each viewfield.

2.7 | Reagents

PD0325901 (FUJIFILM Wako Pure Chemical Corporation), HCQ (Selleck Chemicals LLC), Compound C (FUJIFILM Wako Pure Chemical Corporation), TPA (12-O-Tetradecanoylphorbol-13-Acetate, Sigma Aldrich), SCH772984 (Selleck Chemicals), 2-DG (Sigma Aldrich), and Compound C (Selleck Chemicals) were used.

2.8 | Image Analysis

PDAC organoids expressing EKAREN5-gl-NLS and AMPKAR-EV were segmented by ImageJ plugins Trackmate [47] and Cellpose [48], respectively. The segmented cells were subjected to a cluster analysis using Matlab software (Mathworks) where cells within 20 μm of Euclidean distance are recognized as single organoids.

2.9 | Quantitative Analysis of PDAC Organoids

Organoids were recognized as cell clusters of ≥ 10 cells (Figure 2A). Organoid formation efficiency was calculated as the proportion of the number of organoids among the total number of cell clusters.

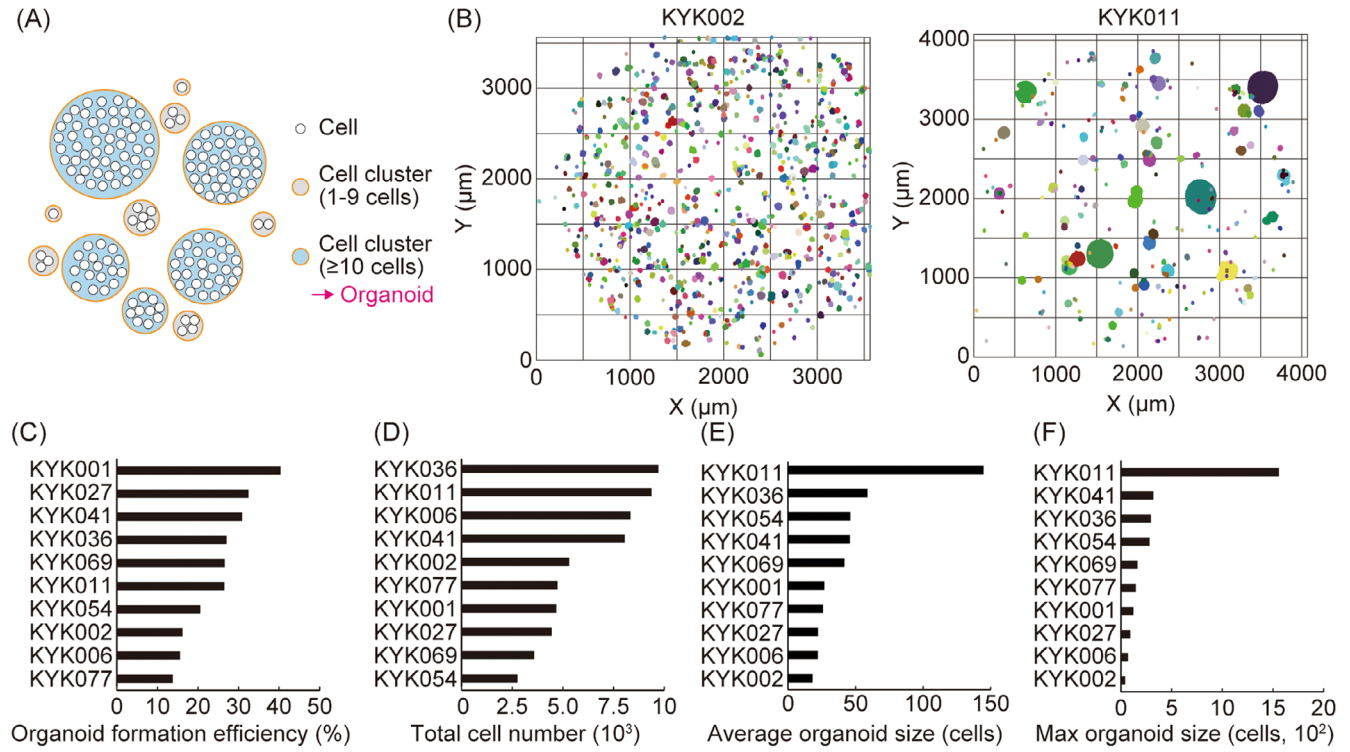

FIGURE 2 | Quantitative evaluation of the growth of PDAC organoid lines. (A) Schematic showing the segmentation of single cells and single organoids. Cells within distances of 20 μm are recognized as cell clusters, and cell clusters of ≥10 cells are recognized as organoids. (B) Spatial mappings of individual organoids in KYK002 (left) and KYK011 (right) organoid lines cultured for 7 days. Colors indicate distinct organoids. (C–F) Organoid formation efficiency (C, see Section 2), the total cell number (D), the average number of cells in organoids (E), and the cell number in the largest organoid observed (F) in the 10 PDAC organoid lines. The organoid lines are ordered from top to bottom in descending order.

2.10 | Statistical Analysis

Excel software (Microsoft) was used for all the statistical analyses. Paired and unpaired Student's *t*-tests were used to statistically examine the differences in ERK activity and its heterogeneity (standard deviation). Data are shown as means ± SD, and a *p*-value <0.05 was considered as statistically significant ($^{*}p<0.05$, $^{**}p<0.01$, $^{***}p<0.001$, n.s., not significant). Linear regression and correlation coefficient (R) were obtained by Excel software.

2.11 | Code Availability

The codes in this study are available from the corresponding author upon reasonable request.

3 | Results

3.1 | Quantitative Live Imaging of ERK and AMPK Kinase Activity in PDAC Patient-Derived Organoids

We used 10 PDAC patient-derived organoids (KYK001–KYK077) with varied morphological features and genetic backgrounds (Figure 1A,B). To comprehensively observe the heterogeneous PDAC cell population, we acquired Z-stack (1200–1500 μm) images of the whole gel area of the PDAC cells by tile-scan of multiple viewfields (49–64 viewfields, 12.7–16.5 mm^2) using a multiphoton microscope equipped with an incubator system though the number of organoid lines is limited by the microscope availability and image acquisition time (10–12 h for each organoid line) (Figure 1C). The patient-derived organoids were transduced with Förster resonance energy transfer (FRET) probes for ERK and AMPK. For ERK activity, we used nucleus-located EKAREN5-gl-NLS, which is a modified version of EKAREN5 [49] designed to reduce the homology of the two fluorescence protein sequences that can potentially cause homologous recombination during retroviral induction [50] (Figure 1D and Figure S1A–C). For AMPK activity, we used a previously reported cytoplasm-located probe, AMPKAR-EV [46] (Figure 1E). We confirmed the expression level of the biosensors does not affect the FRET ratio (FRET/CFP) values (Figure S1D). Furthermore, we used a kinase-dead negative control biosensor, EKAREN5-gl-NLS-TA (Figure S1E) to pharmacologically test the dynamic ranges of EKAREN5-gl-NLS and AMPKAR-EV (Figure S1F,G). Because of the autofluorescence of Compound C (Figure S1G), we performed FLIM imaging of KYK054 cells expressing the ERK and AMPK probes and confirmed their responses to the activators and inhibitors (Figure S1H–K).

3.2 | Quantitative Evaluation of Heterogeneous Growth Potentials of Human PDAC Cells

We performed a single-cell segmentation using ImageJ plugins, Trackmate [47, 51] for nucleus-located EKAREN5-gl-NLS and Cellpose [48] for cytoplasm-located AMPKAR-EV. Furthermore,

we segmented individual cell clusters by a cluster analysis where cells within 20 μm distances are segmented as a single cell cluster (Figure 2A). In this study, we defined "organoids" as cell clusters of ≥ 10 cells. The human PDAC organoids cultured for 7 days showed heterogeneous growth potentials (Figure 2B and Figure S2). For instance, KYK002 organoids were homogeneous in size while KYK011 showed organoids of various sizes. We evaluated the proportion of organoids among the total cell clusters, which we hereafter call "organoid formation efficiency." In line with previous studies [52], only a small fraction of the cells formed organoids (Figure 2C). Notably, the overall cell growth was not necessarily correlated with the cell numbers of the largest organoid in each organoid line, the average cell number of organoids, nor the organoid formation efficiency, highlighting the advantage of our quantitative approach (Figure 2C–F). Indeed, despite the distinctive difference between KYK002 and KYK011 in their organoid size, the two organoid lines showed similar organoid formation efficiency. This suggests that the KYK011 cell population is mainly occupied by fewer but highly proliferative organoids. The common KRAS G12V mutation in the two organoid lines (Figure 1B) suggests organoid growth is regulated by multiple factors not limited to KRAS gene mutation. Because of these varied growth patterns, we evaluated the growth of the organoid lines by four distinct standards: total cell number, average organoid size, the cell number of the largest organoid, and the organoid formation efficiency (Figure 2C–F). Together, our non-selective and automated live imaging approach provided us with multiple readouts to quantitatively evaluate the heterogeneous growth potential of human PDAC cells.

3.3 | ERK Activity Contributes to the Early Phase of Human PDAC Organoid Growth

Next, we related the heterogeneous cell growth of PDAC cells to the ERK signal activity. The spatial mapping of ERK activity in the 10 patient-derived organoid lines showed varied ERK activity patterns (Figure 3A and Figure S3). We did not find obvious spatial differences of ERK activity in the Matrigel (e.g., center vs. periphery) (Figure 3A and Figure S3), but we found the activity is fluctuating by time in three organoid lines, which may contribute to the spatial heterogeneous of ERK activity (Figure S4). Our quantitative analysis (Figure 2A) revealed the ERK activity dynamics from multiple perspectives. For example, KYK002 and KYK011 showed high average ERK activity, while KYK077 showed the lowest average activity (Figure 3B). In contrast, the degree of heterogeneity was high in KYK011 and KYK077, and intermediate in KYK002. Although neither the average ERK activity nor its heterogeneity was correlated with the organoid formation efficiency (Figure 3C) or the overall cell growth (Figure S5A), both the average ERK activity and its heterogeneity were positively correlated with the average organoid size (Figure 3D, $R = 0.56$ and $R = 0.51$) and the size of the largest organoid (Figure S5B, $R = 0.57$ and $R = 0.62$). This highlights the significance of observing individual organoids rather than indirectly measuring their growth by other methods such as MTT assay. Additionally, we found that ERK activity is relatively homogeneous in cells comprising each organoid compared to organoid-to-organoid ERK activity heterogeneity, suggesting the involvement of cell–cell interactions and local paracrine signals (Figure 3E). Furthermore, examination of ERK activity in individual organoids revealed organoids with lower cell numbers tend to have higher ERK activity in some organoid lines, KYK001, 006, 011, 027, and 041 (Figure 3F and Figure S6). This suggests that high ERK activity contributes to early-stage organoid growth rather than late-stage growth.

3.4 | Inverse Correlation of ERK and AMPK Activity in Human PDAC Organoid

To investigate the role of autophagy signaling pathway, we monitored AMP-activated protein kinase (AMPK) activity using AMPKAR-EV [46]. As observed in ERK activity, AMPK activity was highly heterogeneous between individual cells, organoids, and patients (Figure 4A,B, and Figure S7). We found that AMPK activity is higher at the periphery in some organoid lines including KYK001, KYK036, and KYK054 (Figure 4A and Figure S7). The overall average AMPK activity was high in KYK077, intermediate in KYK027, and low in KYK036. In contrast, the degree of heterogeneity was high in KYK041 and low in KYK069 cells, suggesting the AMPK activity and its heterogeneity are differentially regulated in the 10 organoid lines (Figure 4B). As observed in ERK activity, single-cell AMPK activity was also fluctuating by time in the three organoid lines (Figure S8). The more intense fluctuations of AMPK activity than those of ERK activity (Figure S4) may explain the high spatial heterogeneity. Organoid formation efficiency was mildly correlated with AMPK activity but not its heterogeneity (Figure 4C, $R = 0.39$ and $R = 0.021$). The average organoid size was negatively correlated with AMPK activity, which is in sharp contrast to the positive correlation observed with ERK activity (Figure 3D and Figure 4D, $R = -0.63$). Consistently, we found strong negative correlations between the average AMPK activity and the total cell number or the largest organoid size (Figure S9A,B, $R = -0.88$ and $R = -0.61$). On the other hand, the heterogeneity of AMPK activity was not correlated with the organoid formation efficiency, the average organoid size, the total cell number, or the largest organoid size (Figure 4C,D and Figure S9A,B). This inverse correlation of AMPK activity and organoid growth suggests the metabolic adaptation of the PDAC organoids to the nutrient conditions. As seen in ERK activity, AMPK activity showed low heterogeneity inside each organoid compared to the overall heterogeneity between organoids (Figure 4E). In sharp contrast to ERK activity, large organoids tend to have higher AMPK activity (Figure 4F and Figure S10), which suggests a role of AMPK activity in the late-stage growth of organoids while ERK activity is important in the early-phase growth of organoids. Supporting this, the average ERK and AMPK activities were inversely correlated (Figure 4G, $R = -0.65$). These results show the phase dependency of organoid growth on the two signaling pathways, ERK and AMPK.

3.5 | The Emergence of Resistant Human PDAC Organoids by Long-Term Pharmacological Inhibition of ERK

Given the heterogeneity of ERK and AMPK activities, we pharmacologically inhibited ERK and autophagy to examine their effects on organoid growth. The PDAC cells were cultured with or without a MEK inhibitor, PD0325901, for 13 days. For each condition,

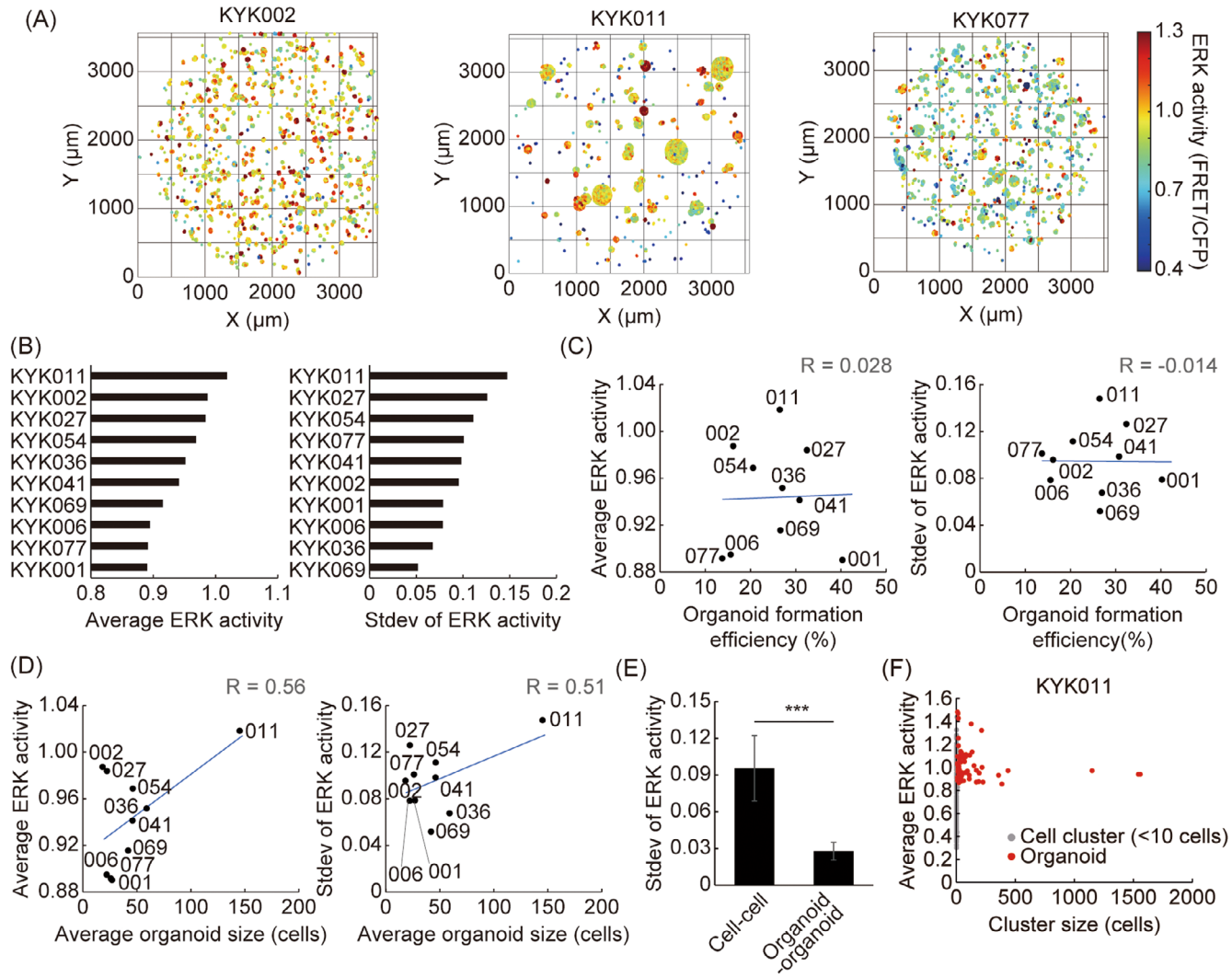

FIGURE 3 | Spatial ERK activity dynamics in PDAC organoid lines. (A) Spatial mappings of single-cell ERK activity (FRET/CFP) in KYK002 (left), KYK011 (middle), and KYK077 (right) were cultured for 7 days. (B) Average (left) and standard deviation (right) of ERK activity (FRET/CFP) of the 10 PDAC organoid lines. (C, D) The association of organoid formation efficiency (C) or average organoid size (D) with average ERK activity (FRET/CFP) (left) and its standard deviation (right). Numbers indicate the serial number of KYK organoid lines. Linear regression and correlation coefficient (*R*) are shown. (E) Standard deviation of ERK activity of single cells (cell–cell) and that of average ERK activity of single organoids (organoid–organoid). Values are shown as mean ± SD. *p* Value is shown by a two-tailed unpaired Student's *t*-test. (F) The association between average ERK activity and the number of cells in the individual cell clusters of KYK011. Red and gray dots indicate organoids (≥ 10 cells) and cell clusters of 9 or fewer cells, respectively. ***$p < 0.001$.

a total of 25 (5 × 5) view fields (6.47 mm^2) were observed by a two-photon microscope and the drug effect was evaluated by (1) the total cell number (Figure 5A), (2) the total number of organoids (Figure 5B), and (3) the size of the largest organoid (Figure 5C) because the organoid formation efficiency and the average organoid size reflect the survived cell population rather than the inhibitory effect of the drug. As a result, PD0325901 showed varied effects on individual organoid growth. While the growth of KYK001, KYK002, KYK006, KYK027, KYK054, and KYK077 cells was almost completely blocked as indicated by the low values in the three growth indicators (Figure 5A–C) and the spatial mappings (Figure 5D and Figure S11), KYK036 and KYK041 cells showed a large organoid comparable to a organoid in the negative control organoid even in the presence of the inhibitor, and KYK011 and KYK069 showed a contradictory promotion of cell growth. Intriguingly, despite the decreased ERK activity immediately after the MEK inhibitor treatment (Figure 5E), the long-term (13 days) inhibitor-treated groups showed comparable or even higher ERK activity than the control groups (Figure 5F). We revisited the same observation area at Day 0, 3, 6, 9, and 13 in KYK041 and found the ERK activity is maintained even in the presence of the MEK inhibitor for a long term at a comparable level to the control group (Figure S12). This resistance suggests a possible decrease in phosphatase activity or activation of other relevant kinases such as ERK5 [53].

3.6 | Resistance of Small PDAC Organoids Against Autophagy Inhibitor

Next, we tested an autophagy inhibitor, HCQ. We confirmed that HCQ does not affect intensity-based ratiometric analysis

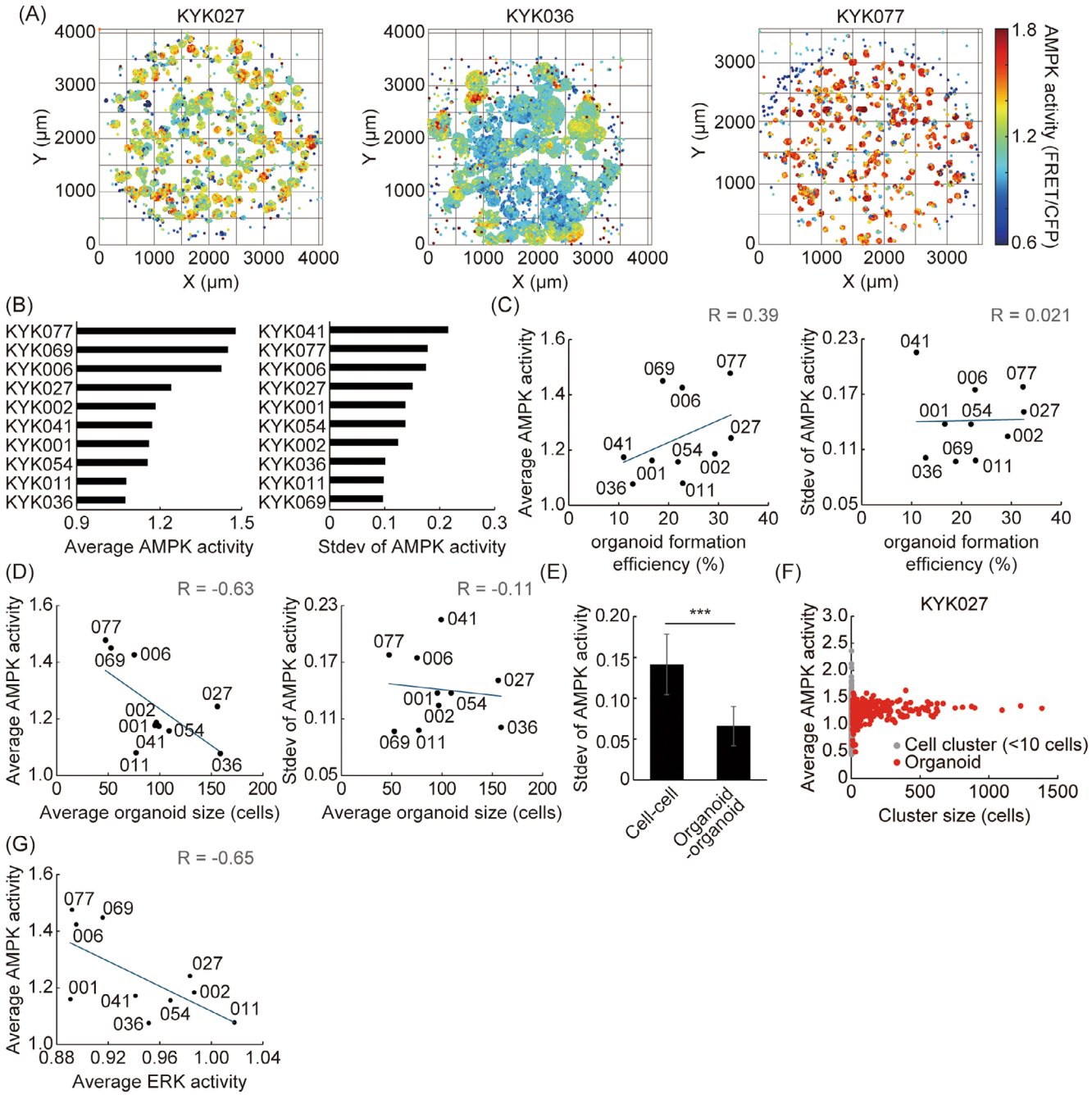

FIGURE 4 | Spatial single-cell AMPK activity dynamics in human PDAC organoid lines. (A) Spatial mappings of single-cell AMPK activity (FRET/CFP) in KYK027 (left), KYK036 (middle), and KYK077 (right) organoid lines cultured for 13 days. (B) Average (left) and standard deviation (right) of AMPK activity (FRET/CFP) of organoids in the 10 PDAC organoid lines. (C, D) The association of organoid formation efficiency (C) or average organoid size (D) with average AMPK activity (FRET/CFP) (left) and the standard deviation (right). Numbers indicate the serial number of KYK organoid lines. Linear regression and correlation coefficient (R) are shown. (E) Standard deviation of AMPK activity of single cells (cell–cell) and that of average AMPK activity of single organoids (organoid–organoid). Values are shown by mean ± SD. p Value was obtained by two-tailed unpaired Student's t-test. (F) The association of average AMPK activity and the number of cells in the individual cell clusters of KYK011. Red and gray dots indicate organoids (≥ 10 cells) and cell clusters of lower than 10 cells, respectively. (G) The association of ERK activity with AMPK activity. Numbers indicate the serial number of KYK organoid lines. Linear regression and correlation coefficient (R) are shown. ***$p < 0.001$.

using EKAREN5-gl-NLS-TA (Figure S1L). By two-photon microscope observation, we found HCQ invariably suppressed the overall cell growth in all 10 PDAC organoid lines examined (Figure 6A–C and Figure S13). HCQ-treated PDAC cells did not show large organoids as seen in PD0325901-treated PDAC cells (Figure 6C). However, we found small organoids persisted even in the presence of HCQ as indicated by the relatively high number of organoids compared to that in PD0325901-treated cells (Figure 5B and Figure 6B). This was consistent with the spatial mapping analysis, showing small cell clusters even under HCQ treatment (Figure 6D and Figure S13). Consistently, repetitive observations of the same area in KYK054 revealed the surviving cells persisted evading cell death and partially showing proliferative capacity (Figure S14). AMPK activity in the organoids that survived under

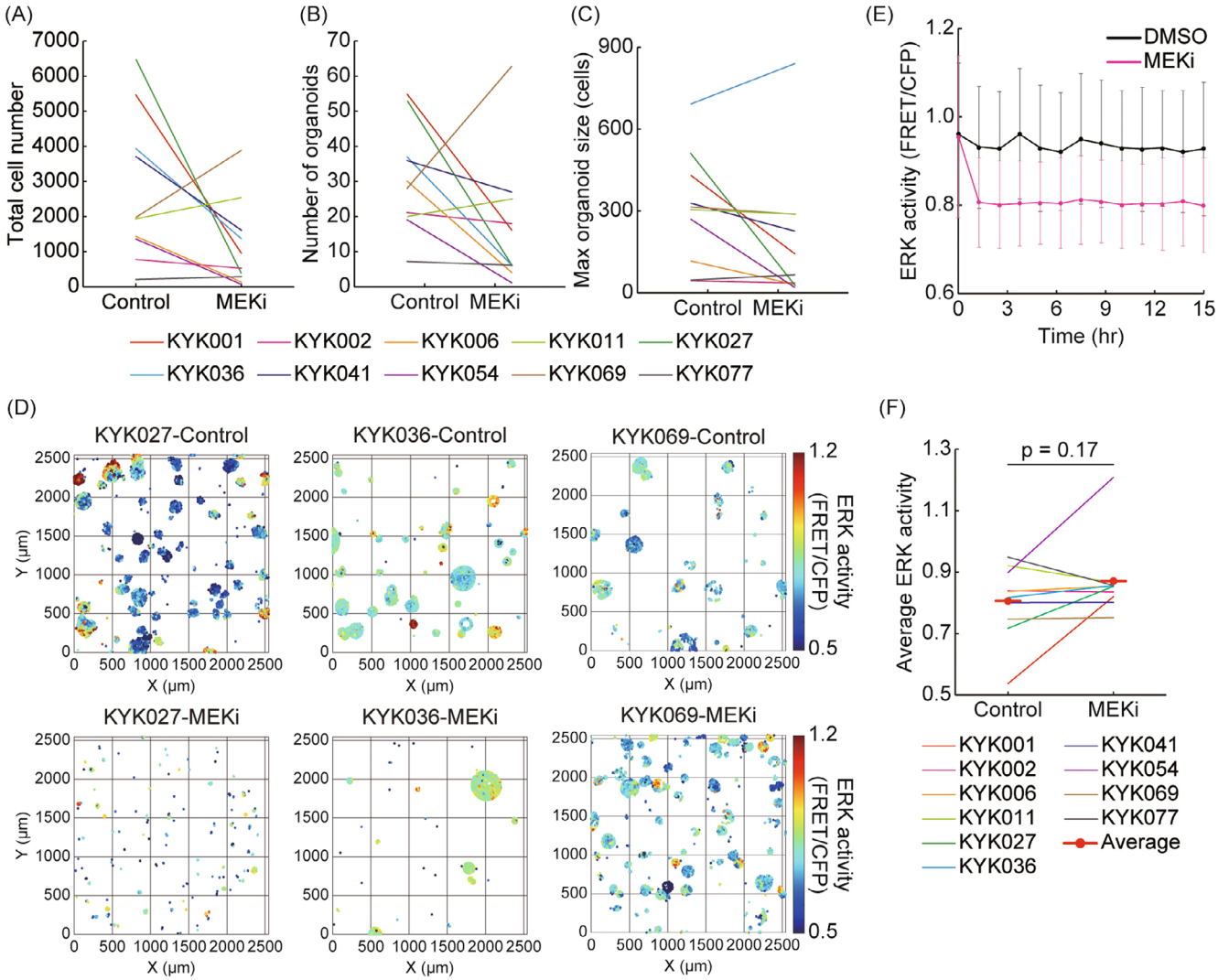

FIGURE 5 | The efficacy of MEK inhibitor treatment in human PDAC organoid lines. (A–C) The total cell number (A), the number of organoids (B), and the number of cells in the largest organoid (C) in the DMSO or 200 nM PD0325901-treated PDAC organoids in the 10 organoid lines. (D) Spatial mappings of single-cell ERK activity (FRET/CFP) in KYK027 (left), KYK036 (middle), and KYK069 (right) organoid line treated with DDW (top) or 200 nM PD0325901 (bottom) for 13 days. (E) Time series of average ERK activity (FRET/CFP) of DMSO or 200 nM PD0325901-treated KYK054 cells. Data are shown by mean ± SD. (F) Average ERK activity (FRET/CFP) of DMSO or 200 nM PD0325901-treated PDAC organoids in the 10 organoid lines. The average of the 10 organoid lines is indicated by red thick bars. *p* Value was obtained by two-tailed paired Student's *t*-test.

HCQ treatment was significantly reduced, which suggests that the growth suppression is attributed to the reduced AMPK activity and the resistance occurs downstream of AMPK (Figure 6D,E and Figure S13). We compare the effect of HCQ with an AMPK inhibitor, Compound C, and found both of the drugs show similar anti-tumor effects in individual overall cell growth and organoid formation (Figure S15), which suggests the anti-tumor effect of HCQ is mediated by AMPK activity inhibition. These distinct effects of HCQ on small and large organoids support the idea that AMPK activity plays a role in late-phase organoid growth.

3.7 | Synergistic Growth Inhibition of PDAC Organoids by MEK Inhibitor and HCQ

Given the distinct functions of the MEK inhibitor and autophagy inhibitor, we tested a combination treatment of PD0325901 and HCQ by confocal microscope observation. The PDAC organoids were cultured for 6 days before treatment to examine their effects on mature organoids. The combination treatment significantly suppressed the growth of most human PDAC organoid lines compared to PD0325901 or HCQ treatment alone, as indicated by the total cell number (Figure 7A), the number of organoids (Figure 7B), and the cell number of the largest organoid (Figure 7C). Note that we failed to observe KYK069 cells as they lost growth potential during this study. Spatial mappings show significant suppressive effects of the combinatory treatment except in KYK011 and KYK027 (Figure 7D and Figure S16). Interestingly, AMPK activity was not reduced by the combination treatment in contrast to HCQ treatment alone (Figure 6E and Figure 7E), which suggests a possible compensatory mechanism where MEK inhibition leads to the activation of AMPK. These results show the combinatory inhibition of the cell growth signal and autophagy signal has a synergistic, or at least an additive effect on a wide range of human PDAC organoid lines.

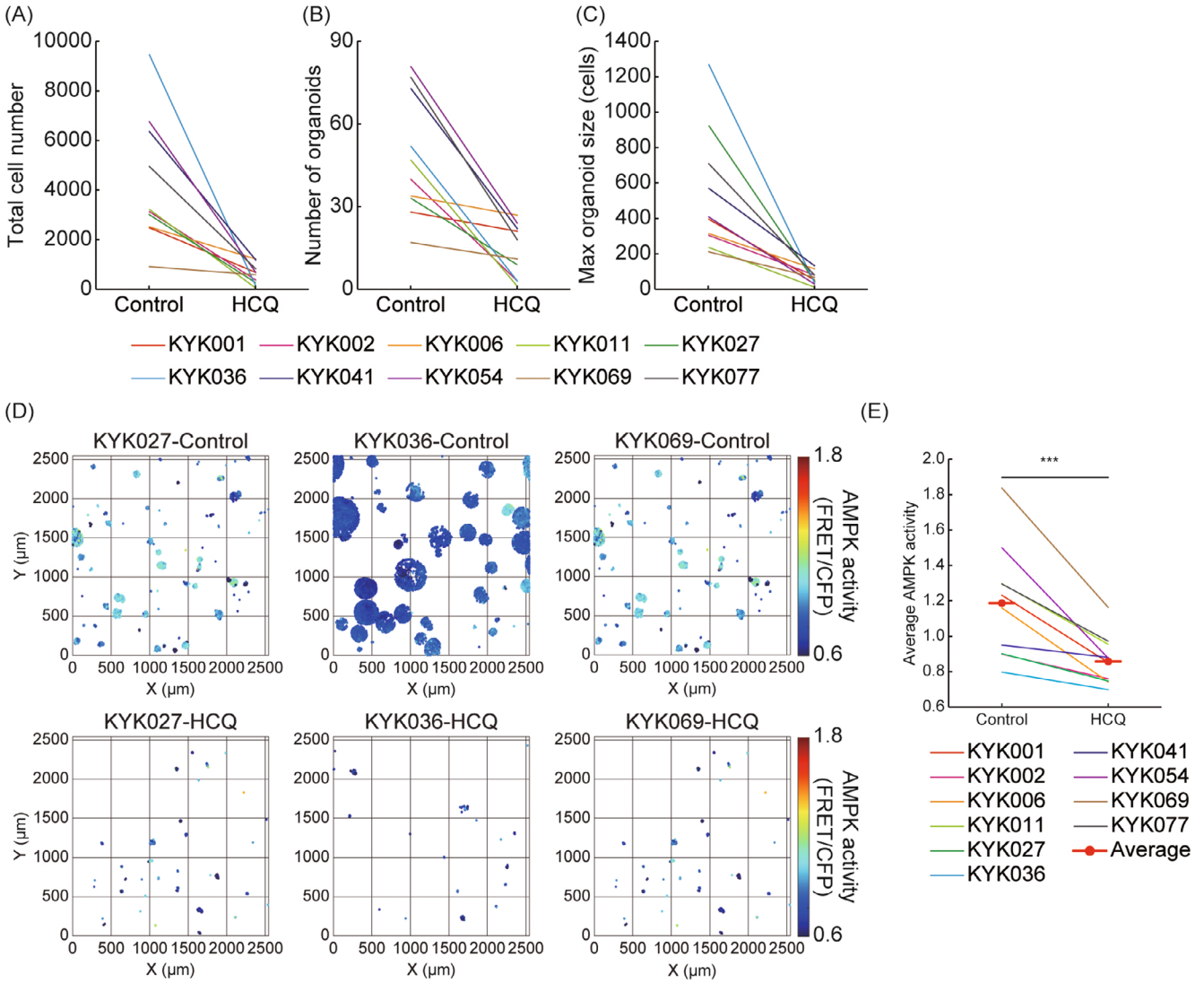

FIGURE 6 | The efficacy of autophagy inhibitor treatment in human PDAC organoid lines. (A–C) The total cell number (A), the number of organoids (B), and the number of cells in the largest organoid (C) in the DDW or 50 μM hydroxychloroquine (HCQ)-treated PDAC organoids in the 10 organoid lines. (D) Spatial mappings of single-cell AMPK activity (FRET/CFP) in KYK027 (left), KYK036 (middle), and KYK069 (right) organoid line treated with DDW (top) or 50 μM HCQ (bottom) for 9 days. (E) Average AMPK activity (FRET/CFP) of DDW or 50 μM HCQ-treated PDAC organoids in the 10 organoid lines. The average of the 10 organoid lines is indicated by red thick bars. *p* Value was obtained by two-tailed unpaired Student's *t*-test. ***$p < 0.001$.

4 | Discussion

Cancer patient-derived organoid culture represents an experimental model that mimics cancer cells in patients and preserves the genomic and transcriptomic profile. However, methodologies to understand the spatiotemporal cancer heterogeneity have yet to be established. Here, we employed a comprehensive live imaging approach to observe the heterogeneous cancer population without selection bias. Our large image dataset provides multi-level tumor heterogeneity from cell–cell, organoid–organoid, and patient–patient levels evaluated from different perspectives: the overall cell number, the number of organoids, the average organoid size, the largest organoid size, and the organoid formation efficiency.

We found ERK activity becomes lower while AMPK activity becomes higher during organoid growth, which suggests the distinct roles of the cellular growth signal and autophagy signal in the early and late phases. Consistently, while both PD0325901 and HCQ suppressed the overall cell growth, the surviving organoids were different: a small number of large organoids emerged under PD0325901 treatment while a large number of small organoids persisted under HCQ treatment. This result supports studies showing the efficacy of the combination strategy of the growth signal and autophagy pathway inhibitors [24–26]. Compared with other comprehensive approaches such as kinome and RNA-seq analyses, our approaches are limited by the number of target molecules analyzed. However, live imaging approaches benefit in revealing single-cell temporal dynamics such as fluctuating activities (Figures S4 and S8) and tracking the efficacy of drug treatment in the same tumor cells (Figures S12 and S14). Our comprehensive evaluation of heterogeneous tumor cell proliferation and underlying kinase activities will provide a new insight

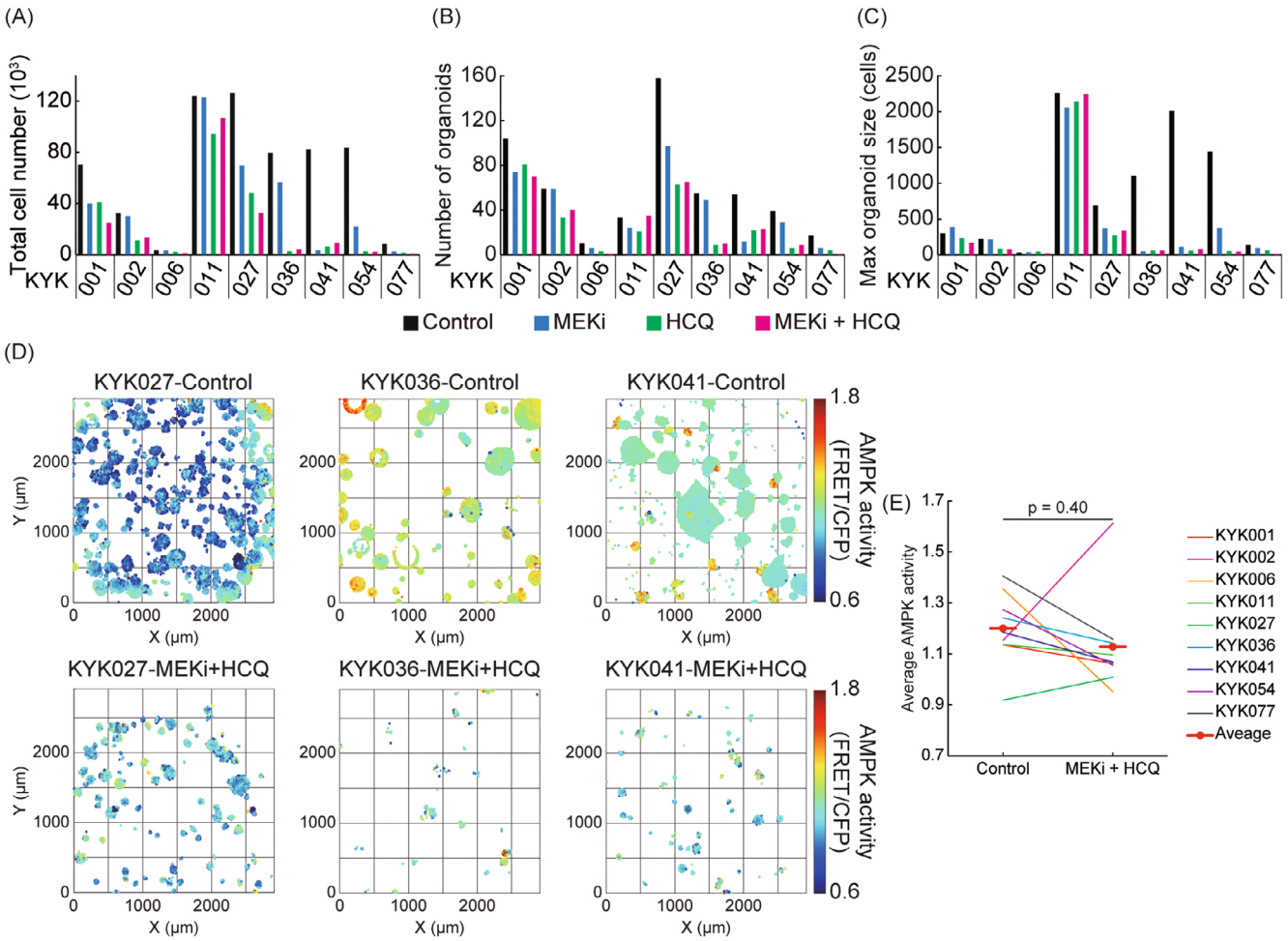

FIGURE 7 | The efficacy of combination of MEK inhibitor and autophagy inhibitor treatment in human PDAC organoid lines. (A–C) The total cell number (A), the number of organoids (B), and the number of cells in the largest organoid (C) in the DMSO and DDW (black) or 200 nM PD0325901 (blue), 50 μM hydroxychloroquine (HCQ) (green), or the combination of PD0325901 and HCQ (red)-treated PDAC organoids in the 10 organoid lines. Numbers indicate the serial number of KYK organoid lines. (D) Spatial mappings of single-cell AMPK activity (FRET/CFP) in KYK027 (left), KYK036 (middle), and KYK041 (right) organoid line treated with DDW and DMSO (top) or 200 nM PD0325901 and 50 μM HCQ (bottom) for 7 days. (E) Average AMPK activity (FRET/CFP) of DMSO and DDW or 200 nM PD0325901 and 50 μM HCQ-treated PDAC organoids in the 9 organoid lines. The average of the 9 organoid lines is indicated by red thick bars. *p* Value was obtained by two-tailed paired Student's *t*-test.

into the current evaluation of drug efficacy such as IC50 and the realization of personalized medicine that eradicates the whole cancer cell population.

Together, our study provides quantitative cellular and molecular dynamics during the growth of organoids and the treatment to anti-cancer drugs. In conjunction with further advancement of single-cell omics studies especially spatial transcriptomics, live imaging will play an important role in understanding the temporal dynamics of cancer heterogeneity for the achievement of personalized medicine for individual cancer patients.

Author Contributions

Shoko Tsukamoto: data curation, formal analysis, funding acquisition, investigation, methodology, writing – original draft, writing – review and editing. **Ye Huaze:** investigation, methodology, writing – review and editing. **Zhang Weisheng:** investigation, methodology, writing – review and editing. **Akihito Machinaga:** conceptualization, methodology, writing – review and editing. **Nobuyuki Kakiuchi:** resources, writing – review and editing. **Seishi Ogawa:** funding acquisition, resources, writing – review and editing. **Hiroshi Seno:** resources, writing – review and editing. **Shigeki Higashiyama:** conceptualization, supervision, writing – review and editing. **Michiyuki Matsuda:** conceptualization, funding acquisition, methodology, supervision, writing – original draft, writing – review and editing. **Toru Hiratsuka:** conceptualization, data curation, formal analysis, funding acquisition, investigation, methodology, project administration, resources, software, supervision, validation, visualization, writing – original draft, writing – review and editing.

Acknowledgments

We would like to sincerely appreciate Dr. Kazuhiro Aoki for kindly sharing resources of his laboratory for the completion of this project. We are grateful to the lab colleagues for their helpful insights and technical assistance, especially to Kanako Takakura, Yukino Inomata, Kyoko Hirano, Marika Hirao, Miyuki Kusakawa, Naoko Nagasaki, Shiho Kakiuchi, and Tomoko Uesugi. Microscope images in this work were

acquired by continuous support and advice from the Kyoto University Live Imaging Center.

Ethics Statement

Approval of the research protocol by an Institutional Reviewer Board: Kyoto University Certified Review Board and Kyoto University Graduate School and Faculty of Medicine, Ethics Committee (G0738).

Informed consent: All informed consent was obtained from the subjects and/or guardians.

Registry and the registration no. of the study/trial: N/A.

Animal studies: N/A.

Conflicts of Interest

S. Tsukamoto, Y. Huaze, Z. Weisheng, N. Kakiuchi, H. Higashiyama, and T. Hiratsuka have no conflict of interest. A. Machinaga is an employee of Eisai Co. Ltd. S. Ogawa is a consultant of Chordia Therapeutics Inc. and Eisai Co. Ltd. S. Ogawa has received grants from Chordia Therapeutics Inc., Eisai Co. Ltd., Otsuka Pharmaceutical Co. Ltd., and Nanpuh Hospital. H. Seno is an Editorial Board member of Cancer Science. S. Higashiyama is an Associate Editor of Cancer Science. M. Matsuda is serving as a scientific advisor to CMIC Pharma Science Co. Ltd.

Data Availability Statement

The data in this study are available from the corresponding author upon reasonable request.

References

1. R. L. Siegel, K. D. Miller, and A. Jemal, "Cancer Statistics, 2018," *CA: A Cancer Journal for Clinicians* 68 (2018): 7–30.

2. Cancer Genome Atlas Research Network, "Integrated Genomic Characterization of Pancreatic Ductal Adenocarcinoma," *Cancer Cell* 32, no. 185–203 (2017): e113.

3. C. J. Halbrook, C. A. Lyssiotis, M. Pasca di Magliano, and A. Maitra, "Pancreatic Cancer: Advances and Challenges," *Cell* 186 (2023): 1729–1754.

4. P. Lito, M. Solomon, L. S. Li, R. Hansen, and N. Rosen, "Allele-Specific Inhibitors Inactivate Mutant KRAS G12C by a Trapping Mechanism," *Science* 351 (2016): 604–608.

5. M. T. Blasco, C. Navas, G. Martín-Serrano, et al., "Complete Regression of Advanced Pancreatic Ductal Adenocarcinomas Upon Combined Inhibition of EGFR and C-RAF," *Cancer Cell* 35 (2019): 573–587.e576.

6. M. Sinn, M. Bahra, T. Liersch, et al., "CONKO-005: Adjuvant Chemotherapy With Gemcitabine Plus Erlotinib Versus Gemcitabine Alone in Patients After R0 Resection of Pancreatic Cancer: A Multicenter Randomized Phase III Trial," *Journal of Clinical Oncology* 35 (2017): 3330–3337.

7. M. J. Moore, D. Goldstein, J. Hamm, et al., "Erlotinib Plus Gemcitabine Compared With Gemcitabine Alone in Patients With Advanced Pancreatic Cancer: A Phase III Trial of the National Cancer Institute of Canada Clinical Trials Group," *Journal of Clinical Oncology* 25 (2007): 1960–1966.

8. J. M. Ostrem, U. Peters, M. L. Sos, J. A. Wells, and K. M. Shokat, "K-Ras(G12C) Inhibitors Allosterically Control GTP Affinity and Effector Interactions," *Nature* 503 (2013): 548–551.

9. G. Bodoky, C. Timcheva, D. R. Spigel, et al., "A Phase II Open-Label Randomized Study to Assess the Efficacy and Safety of Selumetinib (AZD6244 [ARRY-142886]) Versus Capecitabine in Patients With Advanced or Metastatic Pancreatic Cancer Who Have Failed First-Line Gemcitabine Therapy," *Investigational New Drugs* 30 (2012): 1216–1223.

10. P. A. Philip, J. Benedetti, C. L. Corless, et al., "Phase III Study Comparing Gemcitabine Plus Cetuximab Versus Gemcitabine in Patients With Advanced Pancreatic Adenocarcinoma: Southwest Oncology Group-Directed Intergroup Trial S0205," *Journal of Clinical Oncology* 28 (2010): 3605–3610.

11. J. R. Infante, B. G. Somer, J. O. Park, et al., "A Randomised, Double-Blind, Placebo-Controlled Trial of Trametinib, an Oral MEK Inhibitor, in Combination With Gemcitabine for Patients With Untreated Metastatic Adenocarcinoma of the Pancreas," *European Journal of Cancer* 50 (2014): 2072–2081.

12. C. Y. Wilson and P. Tolias, "Recent Advances in Cancer Drug Discovery Targeting RAS," *Drug Discovery Today* 21 (2016): 1915–1919.

13. J. G. Christensen, P. Olson, T. Briere, C. Wiel, and M. O. Bergo, "Targeting Kras(g12c)-Mutant Cancer With a Mutation-Specific Inhibitor," *Journal of Internal Medicine* 288 (2020): 183–191.

14. A. Patgiri, K. K. Yadav, P. S. Arora, and D. Bar-Sagi, "An Orthosteric Inhibitor of the Ras-Sos Interaction," *Nature Chemical Biology* 7 (2011): 585–587.

15. J. Rinehart, A. A. Adjei, P. M. Lorusso, et al., "Multicenter Phase II Study of the Oral MEK Inhibitor, CI-1040, in Patients With Advanced Non-Small-Cell Lung, Breast, Colon, and Pancreatic Cancer," *Journal of Clinical Oncology* 22 (2004): 4456–4462.

16. A. Kasuga, K. Nakagawa, F. Nagashima, et al., "A Phase I/Ib Study of Trametinib (GSK1120212) Alone and in Combination With Gemcitabine in Japanese Patients With Advanced Solid Tumors," *Investigational New Drugs* 33 (2015): 1058–1067.

17. E. Van Cutsem, M. Hidalgo, J. L. Canon, et al., "Phase I/II Trial of Pimasertib Plus Gemcitabine in Patients With Metastatic Pancreatic Cancer," *International Journal of Cancer* 143 (2018): 2053–2064.

18. H. J. Zeh, N. Bahary, B. A. Boone, et al., "A Randomized Phase II Preoperative Study of Autophagy Inhibition With High-Dose Hydroxychloroquine and Gemcitabine/Nab-Paclitaxel in Pancreatic Cancer Patients," *Clinical Cancer Research* 26 (2020): 3126–3134.

19. V. Flemington, E. J. Davies, D. Robinson, et al., "AZD0364 Is a Potent and Selective ERK1/2 Inhibitor That Enhances Antitumor Activity in KRAS-Mutant Tumor Models When Combined With the MEK Inhibitor, Selumetinib," *Molecular Cancer Therapeutics* 20 (2021): 238–249.

20. S. Yang, X. Wang, G. Contino, et al., "Pancreatic Cancers Require Autophagy for Tumor Growth," *Genes & Development* 25 (2011): 717–729.

21. S. Fujii, S. Mitsunaga, M. Yamazaki, et al., "Autophagy Is Activated in Pancreatic Cancer Cells and Correlates With Poor Patient Outcome," *Cancer Science* 99 (2008): 1813–1819.

22. A. Yang, N. V. Rajeshkumar, X. Wang, et al., "Autophagy Is Critical for Pancreatic Tumor Growth and Progression in Tumors With p53 Alterations," *Cancer Discovery* 4 (2014): 905–913.

23. B. M. Wolpin, D. A. Rubinson, X. Wang, et al., "Phase II and Pharmacodynamic Study of Autophagy Inhibition Using Hydroxychloroquine in Patients With Metastatic Pancreatic Adenocarcinoma," *Oncologist* 19 (2014): 637–638.

24. K. L. Bryant, C. A. Stalnecker, D. Zeitouni, et al., "Combination of ERK and Autophagy Inhibition as a Treatment Approach for Pancreatic Cancer," *Nature Medicine* 25 (2019): 628–640.

25. C. G. Kinsey, S. A. Camolotto, A. M. Boespflug, et al., "Protective Autophagy Elicited by RAF→MEK→ERK Inhibition Suggests a Treatment Strategy for RAS-Driven Cancers," *Nature Medicine* 25 (2019): 620–627.

26. C. B. Xavier, K. R. Marchetti, T. B. Castria, D. L. F. Jardim, and G. S. Fernandes, "Trametinib and Hydroxychloroquine (HCQ) Combination Treatment in KRAS-Mutated Advanced Pancreatic Adenocarcinoma: Detailed Description of Two Cases," *Journal of Gastrointestinal Cancer* 52 (2021): 374–380.

27. M. Gong, H. Meng, D. Tan, et al., "Establishment of Organoid Models for Pancreatic Ductal Adenocarcinoma and Screening of Individualized

Therapy Strategy," *Animal Models and Experimental Medicine* 6 (2023): 409–418.

28. I. Romero-Calvo, C. R. Weber, M. Ray, et al., "Human Organoids Share Structural and Genetic Features With Primary Pancreatic Adenocarcinoma Tumors," *Molecular Cancer Research* 17 (2019): 70–83.

29. C. Calandrini, F. Schutgens, R. Oka, et al., "An Organoid Biobank for Childhood Kidney Cancers That Captures Disease and Tissue Heterogeneity," *Nature Communications* 11 (2020): 1310.

30. J. E. Grossman, L. Muthuswamy, L. Huang, et al., "Organoid Sensitivity Correlates With Therapeutic Response in Patients With Pancreatic Cancer," *Clinical Cancer Research* 28 (2022): 708–718.

31. M. Bleijs, M. van de Wetering, H. Clevers, and J. Drost, "Xenograft and Organoid Model Systems in Cancer Research," *EMBO Journal* 38 (2019): e101654.

32. S. I. Choi, A. R. Jeon, M. K. Kim, et al., "Development of Patient-Derived Preclinical Platform for Metastatic Pancreatic Cancer: PDOX and a Subsequent Organoid Model System Using Percutaneous Biopsy Samples," *Frontiers in Oncology* 9 (2019): 875.

33. H. Tiriac, P. Belleau, D. D. Engle, et al., "Organoid Profiling Identifies Common Responders to Chemotherapy in Pancreatic Cancer," *Cancer Discovery* 8 (2018): 1112–1129.

34. E. Driehuis, A. van Hoeck, K. Moore, et al., "Pancreatic Cancer Organoids Recapitulate Disease and Allow Personalized Drug Screening," *Proceedings of the National Academy of Sciences of the United States of America* 116 (2019): 26580–26590.

35. P. O. Frappart, K. Walter, J. Gout, et al., "Pancreatic Cancer-Derived Organoids—A Disease Modeling Tool to Predict Drug Response," *United European Gastroenterology Journal* 8 (2020): 594–606.

36. T. T. Seppälä, J. W. Zimmerman, E. Sereni, et al., "Patient-Derived Organoid Pharmacotyping Is a Clinically Tractable Strategy for Precision Medicine in Pancreatic Cancer," *Annals of Surgery* 272 (2020): 427–435.

37. S. Hyun and D. Park, "Challenges in Genomic Analysis of Model Systems and Primary Tumors of Pancreatic Ductal Adenocarcinoma," *Computational and Structural Biotechnology Journal* 20 (2022): 4806–4815.

38. A. Marusyk, M. Janiszewska, and K. Polyak, "Intratumor Heterogeneity: The Rosetta Stone of Therapy Resistance," *Cancer Cell* 37 (2020): 471–484.

39. U. Ben-David, G. Ha, Y. Y. Tseng, et al., "Patient-Derived Xenografts Undergo Mouse-Specific Tumor Evolution," *Nature Genetics* 49 (2017): 1567–1575.

40. Q. Xu, S. Chen, Y. Hu, and W. Huang, "Single-Cell RNA Transcriptome Reveals the Intra-Tumoral Heterogeneity and Regulators Underlying Tumor Progression in Metastatic Pancreatic Ductal Adenocarcinoma," *Cell Death Discovery* 7 (2021): 331.

41. Y. Mao, J. Shen, Y. Lu, et al., "RNA Sequencing Analyses Reveal Novel Differentially Expressed Genes and Pathways in Pancreatic Cancer," *Oncotarget* 8 (2017): 42537–42547.

42. T. G. Krieger, S. Le Blanc, J. Jabs, et al., "Single-Cell Analysis of Patient-Derived PDAC Organoids Reveals Cell State Heterogeneity and a Conserved Developmental Hierarchy," *Nature Communications* 12 (2021): 5826.

43. J. Peng, B. F. Sun, C. Y. Chen, et al., "Single-Cell RNA-Seq Highlights Intra-Tumoral Heterogeneity and Malignant Progression in Pancreatic Ductal Adenocarcinoma," *Cell Research* 29 (2019): 725–738.

44. Z. Weisheng, J. Nakayama, Y. Inomata, S. Higashiyama, and T. Hiratsuka. "A Sensitive Erk Fluorescent Probe Reveals the Significance of Minimal Egf-Induced Transcription," *Cell Structure and Function* (2024). https://doi.org/10.1247/csf.24070

45. S. Lin, D. Hirayama, G. Maryu, et al., "Redundant Roles of EGFR Ligands in the ERK Activation Waves During Collective Cell Migration," *Life Science Alliance* 5 (2022): e202101206.

46. Y. Konagaya, K. Terai, Y. Hirao, et al., "A Highly Sensitive FRET Biosensor for AMPK Exhibits Heterogeneous AMPK Responses Among Cells and Organs," *Cell Reports* 21 (2017): 2628–2638.

47. D. Ershov, M. S. Phan, J. W. Pylvänäinen, et al., "TrackMate 7: Integrating State-of-the-Art Segmentation Algorithms Into Tracking Pipelines," *Nature Methods* 19 (2022): 829–832.

48. C. Stringer, T. Wang, M. Michaelos, and M. Pachitariu, "Cellpose: A Generalist Algorithm for Cellular Segmentation," *Nature Methods* 18 (2021): 100–106.

49. G. Maryu, M. Matsuda, and K. Aoki, "Multiplexed Fluorescence Imaging of ERK and Akt Activities and Cell-Cycle Progression," *Cell Structure and Function* 41 (2016): 81–92.

50. A. T. Komatsubara, M. Matsuda, and K. Aoki, "Quantitative Analysis of Recombination Between YFP and CFP Genes of FRET Biosensors Introduced by Lentiviral or Retroviral Gene Transfer," *Scientific Reports* 5 (2015): 13283.

51. J. Schindelin, I. Arganda-Carreras, E. Frise, et al., "Fiji: An Open-Source Platform for Biological-Image Analysis," *Nature Methods* 9 (2012): 676–682.

52. L. Huang, A. Holtzinger, I. Jagan, et al., "Ductal Pancreatic Cancer Modeling and Drug Screening Using Human Pluripotent Stem Cell- and Patient-Derived Tumor Organoids," *Nature Medicine* 21 (2015): 1364–1371.

53. A. Tubita, I. Tusa, and E. Rovida, "Playing the Whack-A-Mole Game: ERK5 Activation Emerges Among the Resistance Mechanisms to RAF-MEK1/2-ERK1/2-Targeted Therapy," *Frontiers in Cell and Development Biology* 9 (2021): 647311.

Supporting Information

Additional supporting information can be found online in the Supporting Information section.